Persistent Medium-Range Order and Anomalous Liquid Properties of Al_{1-x}Cu_{x} Alloys

Joongoo Kang, Junyi Zhu, Su-Huai Wei, Eric Schwegler, and Yong-Hyun Kim

Phys. Rev. Lett. **108**, 115901 — Published 13 March 2012

DOI: 10.1103/PhysRevLett.108.115901

Persistent Medium-Range Order and Anomalous Liquid Properties of $Al_{1-x}Cu_x$ Alloys

Joongoo Kang[1], Junyi Zhu[1], Su-Huai Wei[1], Eric Schwegler[2], and Yong-Hyun Kim[3]

[1]National Renewable Energy Laboratory, Golden, Colorado 80401, USA

[2]Lawrence Livermore National Laboratory, Livermore, California 94550, USA

[3]Graduate School of Nanoscience and Technology (WCU), KAIST, Daejeon 305-701, Korea

The development of short-to-medium-range order in atomic arrangements—that is, the aggregation or packing of short-range order (SRO) atomic clusters—has generally been observed in noncrystalline solid systems such as metallic glasses. Whether such medium-range order (MRO) can exist in materials at well above their melting or glass-transition temperature has been a long-standing important scientific challenge. Here, using *ab initio* molecular dynamics simulations, we show that a novel, persistent MRO exists in liquid Al-Cu alloys near the composition of $CuAl_3$. The correlated atomic motions associated with the MRO give rise to a substantially enhanced viscosity in the vicinity of the composition. The component of the MRO liquid state gradually decreases with increasing temperature, and it disappears above a crossover temperature T_{LLC}. The continuous liquid–liquid crossover (LLC) through a percolation-like transition leads to a pronounced heat capacity peak at T_{LLC}.

Liquids are *not* structureless; unlike what they appear to be at first glance, liquid metals in general contain characteristic atomic structures over short ranges. For instance, the icosahedral atomic cluster (Ih13) is one of the most common, locally favored structures in liquid metals and alloys, and represents the tendency to form short-range order (SRO) [1–4]. Understanding liquid structures is important for both fundamental and applied research, because such an atomic ordering can significantly affect the dynamical properties of liquid phases. Recently, a sharp peak in the viscosity isotherms of $Al_{1-x}Cu_x$ alloys was observed at a composition of $CuAl_3$ (i.e., x = 0.25) above the liquidus temperature [5]. The appearance of a viscosity peak in liquid $CuAl_3$ is notable, given that the binary phase diagram of AlCu has a single liquid phase over a wide composition range including x = 0.25 and that no intermetallic solid $CuAl_3$ compound is present [5, 6]. In order to explain the viscosity anomaly in Al-Cu alloys, a hypothetical "microgroupings" of atoms has been proposed [5]. However, the precise nature of the liquid structure and the associated dynamics is largely unknown.

More generally, in the Al-TM liquid alloys (TM = Mn, Fe, Co, Ni, and Cu), the formation of medium-range order (MRO), which is characterized by a pre-peak in the structure factor, has been reported based on high-temperature X-ray and neutron diffraction measurements [7–11]. The short-to-medium range order in the Al-TM liquid alloys is remarkable, considering that a large number of Al-based binary or ternary alloys, e.g., Al-Mn [12] and Al-Cu-TM [13], form quasicrystalline (QC) solid phases via a unique packing of atomic clusters [13, 14]. Hence, fundamental studies of anomalous liquid properties of Al-based alloys could provide a new insight into understanding the short-to-long range ordering in QC-forming Al-based systems [11].

The presence of the MRO in the bulk Al-TM liquid alloys raises an intriguing question whether or not such a high degree of order in liquid states can persist when the size of alloys decreases to the nanometer scale. Understanding the role of the liquid surface phases in the structural and dynamical properties of nanoparticles are of particular importance for nanotechnology, because metallic nanoparticles in liquid states are widely used as catalysts in the vapor-liquid-solid growth of nanostructures and for other applications [15–17].

Using *ab initio* molecular dynamics (MD) simulations, we demonstrate that a short-to-medium range order transition based on fivefold SRO clusters occurs in the liquid states of both Al-Cu nanoalloys and bulk alloys at around a composition of $CuAl_3$. We first show that the MRO formation in the liquid surface of $Al_{55-N_{Cu}}Cu_{N_{Cu}}$ clusters leads to anomalous peaks in the calculated viscosity and heat capacity. Next, we generalize the results of the nanoalloys to the case of bulk Al-Cu liquids, and elucidate how an MRO network emerges in the bulk liquid with reduced dimensionality. In this study, total energies were calculated within the generalized gradient approximation (GGA-PBE [18]) to the density functional theory (DFT) as implemented in the VASP package [19]. For MD simulations at constant temperatures, the Nosé thermostat [20] was used, and the time step was chosen to be 3 fs. Heat capacities of nanoalloys were calculated by using the multiple-histogram method [21–23]. The viscosity of a liquid state at a given temperature and composition was calculated from the Stokes-Einstein relation [24, 25] (see Methods in the Supplemental Material [26]).

Figure 1(a) shows the simulated heat capacity $C(N_{Cu}, T)$ of $Al_{55-N_{Cu}}Cu_{N_{Cu}}$ nanoalloys which reveals three distinct states, S, L and L*, in the Al rich region (Cu content up to 33 at. %). Here, S and L denote solid-like and liquid-like states, respectively. These states are

separated by a noticeable peak in the heat capacity, whose position is denoted by a dot in Fig. 1(a). For $N_{Cu} \leq 10$, the heat capacity curve exhibits a single sharp peak at the melting temperature T_m [Fig. 1(b)]. In contrast, for N ranging from 11 to 17, a second heat capacity peak associated with an L*–L crossover (LLC) appears at T_{LLC}, which is substantially higher than T_m [Fig. 1(c)]. The separation of the two peaks, $T_{LLC}-T_m$, is especially large for N = 13–15 in the vicinity of the composition $CuAl_3$. The $Al_{42}Cu_{13}$ exhibits an S-bend in the microcanonical caloric curve near T_m [Fig. S1 in the Supplemental Material], which is characteristic of a first-order-like transition in the nanoclusters [21, 27, 28]. In contrast, the microcanonical caloric curve near T_{LLC} increases monotonically, indicating that the LLC differs from the first-order-like S–L* transition.

The intermediate L* state is characterized by substantially large dynamic viscosity (μ) compared to that of the normal liquid state L. The simulated isotherms of μ for $T_m < T < T_{LLC}$ exhibit a peak at about N = 14, which corresponds to the composition $CuAl_3$ [Fig. 1(d)]. The unprecedented peaks in the heat capacity and the viscosity raise the following questions: (i) How does the structure of the abnormal L* state differ from that of the normal L state? (ii) How does the continuous LLC occur near T_{LLC}? (iii) What is the microscopic origin of the viscosity anomaly at $CuAl_3$ for $T < T_{LLC}$?

From the analysis of the atomic motions in liquid states, we found that the SRO structure in the Al-Cu nanoalloys has a pentagonal arrangement of surface atoms, as shown in the snapshots of $Al_{42}Cu_{13}$ [Fig. 2(a)]. Interestingly, this icosahedral fragment with a fivefold local symmetry has been shown to be favorable in many other bulk liquids such as Pb, Ni, Zr, Fe, and AuSi [1–4]. At a given temperature, the number of the SRO structures

(N_{SRO}) in a nanoalloy exhibits large thermal fluctuations over time because the SRO is a dynamic order with a relatively short lifetime. Therefore, the probability distribution of N_{SRO} (P_{SRO}) is very broad, ranging from N_{SRO} = 0 up to 15, with an average number of 5.9 and 1.6 at T = 850 and 1300 K, respectively [Fig. 2(b)]. We found that $\langle N_{SRO} \rangle$ generally decreases with increasing T.

The liquid surface of the Al-Cu nanoalloys provides an ideal medium for the formation of the SRO clusters. When its density is sufficiently large, the SRO clusters aggregate to form a medium-range order cluster. In an MRO cluster, the pentagonal clusters are connected to each other by sharing an edge or a vertex [Fig. 2(a)]. Schematic diagrams in Fig. 2(a) illustrate the formation of an MRO cluster represented by a connected network of dots. Here, s is the number of the SRO clusters in an MRO cluster and s_{max} denotes the maximum size at a given moment. To quantify the MRO formation, we calculated the ensemble-averaged $\langle s_{max} \rangle$ as a function of N_{SRO} from the MD trajectories of $Al_{42}Cu_{13}$ at T = 850 K. $\langle s_{max} \rangle$ generally increases with increasing N_{SRO}, approaching to the value of N_{SRO} (i.e., perfect clustering). The emergence of the large MRO cluster spanning the surface is analogous to the way in which a percolation cluster is formed through the continuous percolation transition. According to the site-percolation theory for an infinite system [29], the first-order derivative $\kappa = \Delta \langle s_{max} \rangle / \Delta N_{SRO}$ is zero if the filling probability p is smaller than a percolation threshold p_c. At $p = p_c$, κ jumps to a finite value and it gradually decreases with increasing p. We find that the κ of the nanoalloy exhibits a peak at $N_C = 9$, although the peak is broadened due to a significant finite-size effect [Fig. 2(c)]. This indicates that the short-to-medium-range order transition occurs near N_C and that only the

tail of P_{SRO} with $N_{SRO} \geq N_C$ can contribute to the MRO formation [Fig. 2(b)]. Therefore, the liquid state at T = 850 K contains the MRO structure with noticeable probability, while the MRO cluster does not form at T = 1300 K.

We define an *order parameter* P_{MRO} as a probability of having an N_{SRO} above N_C at a given temperature T and composition, i.e., $P_{MRO}(T) = \sum_{N_{SRO} \geq N_C} P_{SRO}(N_{SRO}; T)$. Then, P_{MRO} measures the component of the anomalous liquid state (L_{MRO}), which is negligible for the majority of the temperatures and compositions investigated in Fig. 1(a), except for the region denoted by L*. Noticeable P_{MRO} is achievable only when $\langle N_{SRO} \rangle$ is sufficiently large at a given T and composition. We found that the compositions near $CuAl_3$, corresponding to N_{Cu} = 13–15, has substantially larger $\langle N_{SRO} \rangle$ than other compositions for $T < T_{LLC}$ [Fig. 2(d)]. Figure 2(e) shows the calculated P_{MRO} as a function of T for two representative compositions, N_{Cu} = 10 and 13. At $T > T_{LLC}$, the P_{MRO} is nearly 'zero' for both compositions, because $\langle N_{SRO} \rangle$ is well below N_C = 9 [Fig. 2(d)]. As T is lowered below T_{LLC}, the P_{MRO} of the $Al_{42}Cu_{13}$ starts to gradually increase from zero. Thus, the LLC is a continuous structural crossover of liquid states through the gradual increase of the L_{MRO} component, leading to the heat capacity peak at T_{LLC} [Fig. 1(c)]. In contrast, the P_{MRO} of the $Al_{45}Cu_{10}$ remains small for the entire temperature range. Consequently, the $Al_{45}Cu_{10}$ exhibits the practically featureless heat capacity above T_m [Fig. 1(b)].

The MRO formation in the L* state for N_{Cu} = 13–15 leads to a notable peak in the viscosity isotherms near the composition of $CuAl_3$ [Fig. 1(d)]. Figure 2(f) compares the viscosity μ(T) for two different compositions, N_{Cu} = 10 and 13. For $T > T_{LLC}$, both

nanoalloys are in the normal liquid state L with similar viscosity. In contrast, the viscosity of the $Al_{42}Cu_{13}$ in the L* state at $T < T_{LLC}$ is substantially higher than that of the $Al_{45}Cu_{10}$ in the L state. The difference between the two viscosity curves (filled boxes) clearly shows the additional viscosity component of the L* state due to the gradual increase of L_{MRO} component below T_{LLC}, as quantified by P_{MRO} in Fig. 2(e).

The viscosity anomaly of liquid Al-Cu nanoalloys at the composition of $CuAl_3$ is remarkable, especially considering that a viscosity peak has previously been found in experiments on bulk Al-Cu alloys at the same composition [Fig. 1(e)]. Our simulations also exhibit a peak in the bulk liquid viscosity at T = 1000 K and x_{Cu} = 25% [Fig. 1(e), filled boxes]. Although the simulated peak is not as sharp as it is in the experiment, most likely because of the small supercell size (256 atoms) used in our MD simulations, the overall agreement is excellent. Also, we found that the $Al_{75}Cu_{25}$ liquid alloy exhibits a pre-peak in the simulated partial structure factor [Fig. S3], which is a hallmark of the MRO formation in liquids [7–11]. To identify the constituent SRO structure of the MRO in the simulated liquids, we performed a common neighbor analysis [4, 30]. In this method, pairs of atoms are classified by four Honeycutt–Anderson indices [30] that are determined by the number of nearest-neighbors and their connectivity. For instance, the 1551 pair in the inset of Fig. 3(a) represents a SRO structure with fivefold symmetry, which corresponds to the pentagonal structure in the surface of the Al-Cu nanoalloys. Our common-neighbor analysis for different compositions reveals that the pentagonal cluster with the 1551 pair at the center is the SRO structure responsible for the MRO formation and the viscosity anomaly near x_{Cu} = 25%. Figure 3(b) shows the probability distributions (P_{SRO}) of the number of the

1551 pairs (N_{SRO}) in a supercell for the $Al_{75}Cu_{25}$ and pure Al liquids. As compared to the case of pure Al, the density of the fivefold SRO clusters is significantly enhanced in the presence of Cu atoms due to chemical ordering effects [31].

Figure 3(a) shows a representative snapshot of the Al-Cu alloy at x_{Cu} = 25% and T = 1000 K. Here, only the 1551 pairs and the associated pentagonal rings are displayed from the bulk liquid to illustrate the clustering of the fivefold SRO clusters. The number of the 1551 pairs in the snapshot is 18 per supercell, which is much larger than the average value of N_{SRO} = 11.4 [Fig. 3(b)]. The snapshot illustrates the formation of a network of the fivefold SRO clusters with reduced dimensionality beyond the length scale of a few clusters, representing a *dynamical* MRO, in analogy with the static MRO of metallic glasses [31, 32] and the percolation of the icosahedral clusters near the glass transition temperature of model systems [33]. To estimate a percolation threshold in N_{SRO}, we calculated the percolation probability (P) as a function of N_{SRO} [Fig. 3(c)]. Here, P is a probability of finding at least one MRO structure that connects two opposite boundaries of a cubic supercell. Due to finite-size effect, the percolation probability gets smeared out around the threshold, which is estimated to be N_C = 19.5/supercell. Interestingly, the probability distribution P_{SRO} for x_{Cu} = 25% is highly asymmetric around the peak, with slowly decreasing P_{SRO} for N_{SRO} > 12. This indicates that once SRO clusters are formed, they promote the formation of additional SRO clusters near the already-formed SRO clusters. Such a “cooperativity” of SRO was shown to play decisive roles in determining the general nature of liquid-liquid transitions [34]. Because the threshold density is higher than the average density of the SRO clusters, we expect that a long-range order (LRO)

would not form beyond the length scale of tens of nanometers. However, the *local* density of the SRO clusters can become substantially higher than the average density due to thermal fluctuations [Fig. 3(b)]. Hence, a dynamical MRO network is formed when the local density of the SRO clusters exceeds the threshold, leading to a finite density of the local MRO regions in a sample and subsequently the viscosity anomaly.

In conclusion, we have found that a short-to-medium-range order transition exists in Al-Cu liquid alloys near the composition of $CuAl_3$ that appears to be induced by a percolation-like transition. The microscopic mechanism responsible for the formation of MRO in Al-Cu alloys can be easily generalized to other liquid systems that have a tendency to form a high density of SRO structures. Therefore, the finding of an anomalous liquid state in the Al-Cu nano- and bulk alloy systems may have far-reaching implications for understanding the appearance of liquid structures, the properties of metallic glasses and a wide variety of nanoalloy systems.

Acknowledgement. This work was funded by the U.S. DOE EERE CSP and NREL LDRD programs (DE-AC36-08GO28308). This research used capabilities of the NREL CSC (DE-AC36-08GO28308) and the NERSC (DE-AC02-05CH11231). Y.-H. K. was supported by the WCU program (R31-2008-000-10071-0) through the NRF of Korea.

1. H. Reichert, O. Klein, H. Dosch, M. Denk, V. Honkimäki, T. Lippmann, and G. Reiter, Nature **408**, 839–841 (2000).

2. T. Schenk, D. Holland-Moritz, V. Simonet, R. Bellissent, and D. M. Herlach, Phys. Rev. Lett. **89**, 075507 (2002).

3. N. Jakse and A. Pasturel, Phys. Rev. Lett. **91**, 195501 (2003).

4. T. U. Schülli, R. Daudin, G. Renaud, A. Vaysset, O. Geaymond, and A. Pasturel, Nature **464**, 1174–1177 (2010).

5. N. Yu. Konstantinova, P. S. Popoel', and D. A. Yagodin, High Temperature **47**, 336–341 (2009).

6. M. Hansen, *Constitution of Binary Alloys* (McGraw-Hill, New York, 1958).

7. A. S. Roik, S. N. Galushko, A. V. Samsonnikov, V. P. Kazimirov, V. E. Sokol'skii, and V. A. Shovskii, Russian Metallurgy (Metally) **3**, 201 (2009).

8. Q. Jingyu, B. Xiufang, S. I. Sliusarenko, and W. Weimin, J. Phys.: Condens. Matter **10**, 1211–1218 (1998).

9. S. K. Das, J. Horbach, M. M. Koza, S. Mavila Chatoth, and A. Meyer, Appl. Phys. Lett. **86**, 011918 (2005).

10. J. Brillo, A. Bytchkov, I. Egry, L. Hennet, G. Mathiak, I. Pozdnyakova, D. L. Price, D. Thiaudiere, and D. Zanghi, J. Non-Cryst. Solids **352**, 4008–4012 (2006).

11. O. S. Roik, O. V. Samsonnikov, V. P. Kazimirov, V. E. Sokolskii, and S. M. Galushko, J. Mol. Liquids **151**, 42–49 (2010).

12. D. Shechtman, I. Blech, D. Gratias, and J. W. Cahn, Phys. Rev. Lett. **53**, 1951–1953 (1984).

13. E. Abe, Y. Yan, and S. J. Pennycook, Nature Mater. **3**, 759–767 (2004).

14. A. S. Keys and S. C. Glotzer, Phys. Rev. Lett. **99**, 235503 (2007).

15. R. S. Wagner and W. C. Ellis, Appl. Phys. Lett. **4**, 89 (1964).

16. E. Sutter and P. Sutter, Nano Lett. **8**, 411–414 (2008).

17. B. Cao, A. K. Starace, O. H. Judd, and M. F. Jarrold, J. Am. Chem. Soc. **131**, 2446–2447 (2009).

18. J. P. Perdew, K. Burke, and M. Ernzerhof, Phys. Rev. Lett. **77**, 3865–3868 (1996).

19. G. Kresse and J. Furthmüller, Phys. Rev. B **54**, 11169–11186 (1996).

20. S. Nosé, J. Chem. Phys. **81**, 511 (1984).

21. P. Labastie and R. L. Whetten, Phys. Rev. Lett. **65**, 1567–1570 (1990).

22. P. Chandrachud, K. Joshi, and D. G. Kanhere, Phys. Rev. B **76**, 235423 (2007).

23. J. Kang and Y.-H. Kim, ACS Nano **4**, 1092–1098 (2010).

24. J. P. Hansen and I. R. McDonald, *Theory of Simple Liquids* (Academic, New York, 2006).

25. E. Ko, M. M. G. Alemany, and J. R. Chelikowsky, J. Chem. Phys. **121**, 942 (2004).

26. See Supplemental Material at http://link.aps.org/supplemental/XXX for details on the calculation method and supplemental figures.

27. D. J. Wales and R. S. Berry, Phys. Rev. Lett. **73**, 2875–2878 (1994).

28. J. Kang, S.-H. Wei, and Y.-H. Kim, J. Am. Chem. Soc. **132**, 18287–18291 (2010).

29. D. Achlioptas, R. M. D'Souza, and J. Spencer, Science **323**, 1453–1455 (2009).

30. J. D. Honeycutt and H. C. Andersen, J. Phys. Chem. **91**, 4950–4963 (1987).

31. H. W. Sheng, W. K. Luo, F. M. Alamgir, J. M. Bai, and E. Ma, Nature **439**, 419–425 (2006).

32. D. Ma, A. D. Stoica, and X.-L. Wang, Nature Mater. **8**, 30–34 (2009).

33. T. Tomida and T. Egami, Phys. Rev. B **52**, 3290–3308 (1995).

34. H. Tanaka, Phys. Rev. E **62**, 6968–6976 (2000).

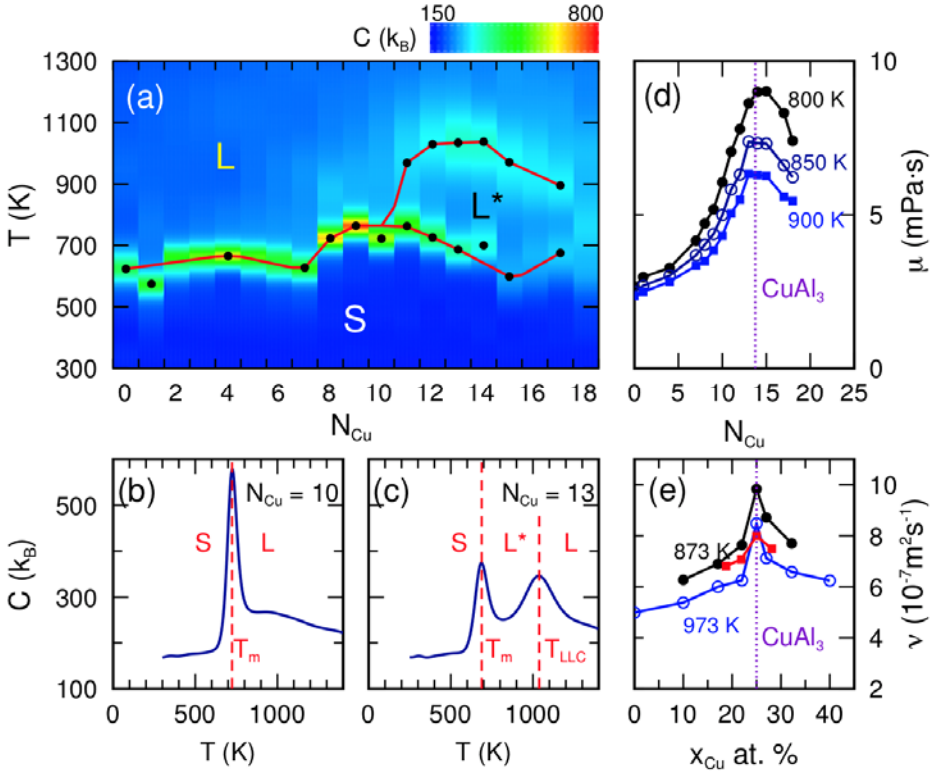

Fig. 1. (color online) Anomalous liquid state of Al-Cu nanoalloys. (a) The color map of the simulated heat capacity $C(N_{Cu}, T)$ of $Al_{55-NCu}Cu_{NCu}$ nanoalloys is shown for a different number of Cu atoms (N_{Cu}) and temperature (T). For some compositions that we did not consider here, we used interpolated values for the map. For each simulated N_{Cu}, the peak positions of the simulated heat capacity are marked by dots. The solid lines connecting the dots represent phase boundaries between two liquid states L and L* and one solid state S. In (b–c), two representative heat capacity curves are shown for N_{Cu} = 10 and 13, respectively. (d) The simulated isotherms of dynamic viscosity (μ) of the Al-Cu nanoalloys are shown for three different temperatures below T_{LLC}. (e) The simulated kinetic viscosities (ν) of bulk Al-Cu alloys at T = 1000 K are shown for compositions around x_{Cu} = 0.25 (filled boxes). The experimental isotherms of the kinetic viscosity (taken from Ref. 5) are also shown for comparison (filled and open circles).

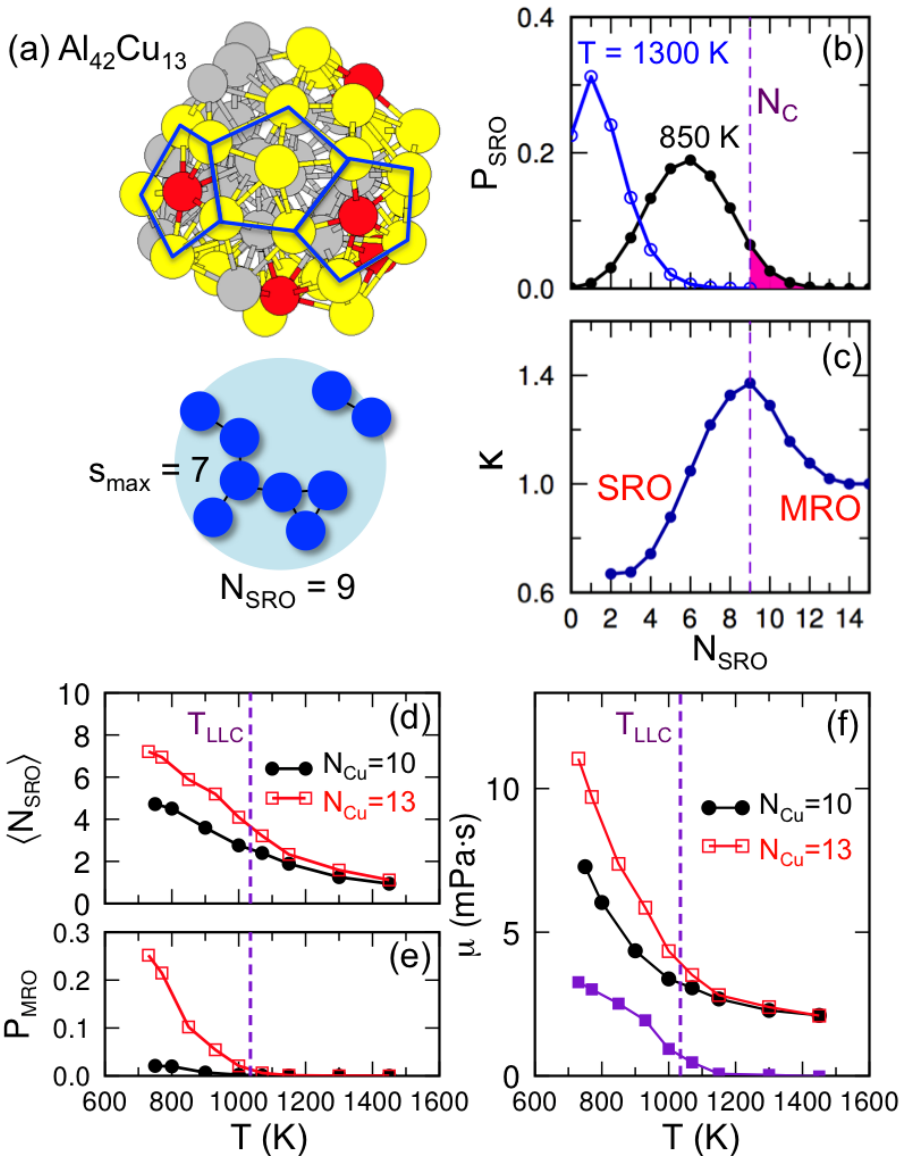

Fig. 2. (color online) Short-to-medium-range surface order. (a) A representative $Al_{42}Cu_{13}$ cluster at T = 850 K is shown. The atoms of the pentagonal SRO clusters (Al: yellow and Cu: red) are highlighted for contrast with the disordered atoms (grey). A schematic figure below illustrates a percolation-like cluster of the SRO structures (represented by dots) with a size s_{max} = 7, forming an MRO cluster. (b) Two representative probability distributions (P_{SRO}) of N_{SRO} are given for the $Al_{42}Cu_{13}$ at T = 850 K (filled circle and black line) and

1300 K (open circle and blue line). (c) The plot of $\kappa = \Delta \langle s_{max} \rangle / \Delta N_{SRO}$ shows a percolation-like transition from the SRO liquid state to the MRO liquid state with a threshold $N_C = 9$. For different compositions (N_{Cu} = 10 and 13) and temperatures, (d) the number of the pentagonal clusters $\langle N_{SRO} \rangle$ and (e) the order parameter P_{MRO} are presented. In (f), the viscosity μ is compared for N_{Cu} = 10 and 13 as a function of temperature above T_m. The difference of the two viscosity curves (filled square) is also given to show the additional component of μ for the L* state below T_{LLC}.

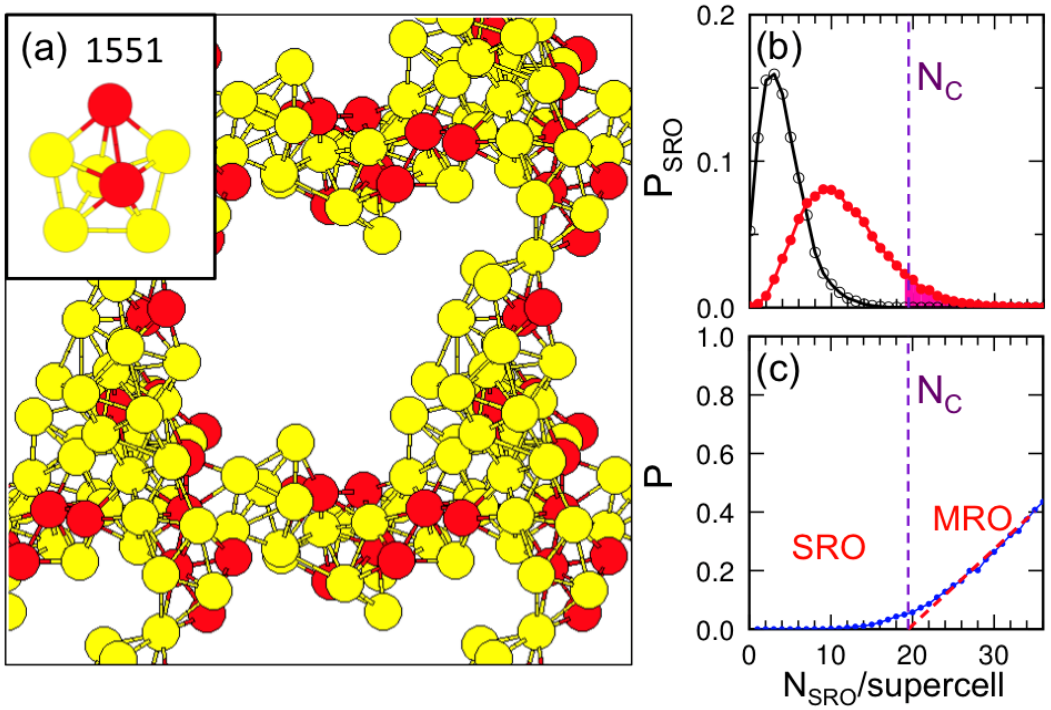

Fig. 3. (color online) Percolated network of the fivefold SRO clusters in bulk liquid $Al_{75}Cu_{25}$. (a) A representative snapshot of the $CuAl_3$ alloy in liquid state at T = 1000 K (Al: yellow and Cu: red). Here, only the 1551 pairs and the associated pentagonal rings are chosen from the bulk liquid to illustrate the clustering of the fivefold SRO structures. The inset shows an isolated SRO structure. (b) Probability distributions (P_{SRO}) of the number of the 1551 pairs (N_{SRO}) in a 256-atom supercell are given for the $Al_{75}Cu_{25}$ (filled circle and red line) and pure Al (open circle and black line) liquid states at T = 1000 K. (c) Percolation probability (P) is shown as a function of N_{SRO}. The vertical dashed lines in (b–c) denote the estimated percolation threshold.